Applied Nanoscience
https://doi.org/10.1007/s13204-018-0907-5

ORIGINAL ARTICLE

Shape- and size-controlled superparamagnetic iron oxide nanoparticles using various reducing agents and their relaxometric properties by Xigo acorn area

Shahid Ali[1] · Safyan A. Khan[1] · Zain H. Yamani[1] · Muhammad T. Qamar[2] · Mohamed A. Morsy[3] · Sadaf Sarfraz[4]

Received: 10 October 2018 / Accepted: 26 October 2018

Abstract

Superparamagnetic iron oxide nanoparticles (SPIONs) were investigated owing to their potential relaxometric properties for magnetic resonance imaging (MRI) applications. For this purpose, shape- and size-controlled SPIONs were prepared using various reducing agents via a facile chemical coprecipitation method. The optimization of reaction parameters such as stirring rate, temperature, reaction time, and pH was carried out to study the particle's growth, size, and shape of nanoparticles (NPs). Transmission electron microscopy (TEM) images reveal that the spherical (9.1 ± 1.5 nm)- and cubic (11.7 ± 1.8 nm)-shaped NPs were attained using NH_4OH and NaOH as reducing agents, respectively. X-ray diffraction (XRD) analysis of as-synthesized SPIONs shows the formation of magnetite (Fe_3O_4) phase having cubic inverse spinel structure. The various oxidation states of Fe were investigated via X-ray photoelectron spectroscopy (XPS) by analyzing Fe 2*p* spectra of SPIONs. The magnetic character and chemical stability of SPIONs were monitored in the synthetic seawater (SW) having salinity 36.03 g L^{-1}; which is the critical requirement for oil reservoir applications. Spin–spin (T_2) relaxation signals were attained using miniaturized Acorn Area analyzer to determine the relaxometric properties. The transverse relaxivities (r_2) for MNP–NH_4OH (41.0 mM^{-1} s^{-1}) and MNP–NaOH (28.5 mM^{-1} s^{-1}) were 2.11 and 1.47 times higher than MNP–KOH (19.4 mM^{-1} s^{-1}), respectively. This study affirms that by controlling the reaction parameters, we can selectively design Fe_3O_4 NPs of desired size and shape, which give enhanced T_2-relaxation and excellent relaxivity properties in SW for potential MRI applications associated with oil reservoirs.

Keywords SPIONs · Reducing agents · T_2-relaxation · Xigo Acorn area · Relaxometric properties

Introduction

Superparamagnetic iron oxide nanoparticles (SPIONs) have received substantial interest owing to their potential applications in the field of magnetic storage (Liu et al. 2005), catalysis (Wu et al. 2009; Gawande et al. 2013), electrocatalysis (Mitra et al. 2006; Odagawa et al. 2007), bimolecular separation (Moeser et al. 2002; Ditsch et al. 2005), and biomedical field, e.g., hyperthermia treatments (Shi et al. 2009; Jiang et al. 2014), targeted drug delivery (Kim et al. 2008b; Maeng et al. 2010), and contrast agents for magnetic resonance imaging (MRI) (Wang et al. 2010). In the past 2 decades, researchers extensively investigated SPIONs as contrast agents for biomedical imaging. Recently, hydrophilic and hydrophobic SPIONs have also been reported as contrast agents for MRI of the oil reservoirs (Chi et al. 2016; Zhang and Daigle 2017). However, the efficiency/contrasting

Electronic supplementary material The online version of this article (https://doi.org/10.1007/s13204-018-0907-5) contains supplementary material, which is available to authorized users.

✉ Shahid Ali
shali@kfupm.edu.sa

✉ Safyan A. Khan
safyan@kfupm.edu.sa

[1] Center of Research Excellence in Nanotechnology, King Fahd University of Petroleum and Minerals, Dhahran 31261, Saudi Arabia

[2] Department of Chemistry, Forman Christian College (A Chartered University), Ferozepur Road, Lahore 54600, Pakistan

[3] Department of Chemistry, King Fahd University of Petroleum and Minerals, Dhahran 31261, Saudi Arabia

[4] Department of Chemistry, Lahore Garrison University, Lahore, Pakistan

Published online: 03 November 2018

ability of these nano-contrast agents remains a challenging area of research.

The contrasting ability of MRI contrast agents is conventionally represented by longitudinal (r_1) and transverse (r_2) relaxivities, which can be evaluated from spin–lattice (T_1) relaxation and spin–spin (T_2) relaxation, respectively. The positive contrast agents enhance T_1-relaxation and provide a brighter image, while negative contrast agents increase the T_2-relaxation and deliver a darker image in MRI (Li et al. 2012). It is well known that T_2-relaxation signal depends on the size and shape homogeneity of NPs; smaller size delivers higher r_2 value (Gao et al. 2016). Therefore, the current research work is focused on investigating the capability of size- and shape-controlled magnetite (Fe_3O_4) NPs as T_2-contrast agents by computing r_2-relaxivity. For such applications, the importance of finely tuned size- and shape-controlled SPIONs is crucial.

Various synthesis protocols such as thermal decomposition (Unni et al. 2017), hydrothermal (Kolen'ko et al. 2014), solvothermal (Patsula et al. 2016), thermolysis (Cha et al. 2010), microemulsion (Okoli et al. 2012), polyol (Abbas et al. 2014), and coprecipitation method (Yazdani and Seddigh 2016; Khan et al. 2017) have been adopted to control the size and shape of SPIONs. Amongst these, coprecipitation is one of the most convenient, widely adopted, and commercially viable methods for aqueous phase synthesis of magnetite NPs. Moreover, coprecipitation can be performed at a relatively low temperature within short reaction time. The synthesis involves coprecipitation of Fe^{3+} and Fe^{2+} (2:1) in the presence of a reducing agent under an inert atmosphere to produce magnetite (Fe_3O_4) NPs based on chemical equation (1) (Roth et al. 2015):

$$2\,Fe^{3+} + Fe^{2+} + 8\,OH^- \rightarrow Fe_3O_4 + 4\,H_2O. \quad (1)$$

To achieve the distinctive characteristics of magnetite NPs, various reducing agents such as NH_4OH (Tajabadi and Khosroshahi 2012), KOH (Du et al. 2009), NaOH (Sayar et al. 2006), and $(C_2H_5)_4NOH$ (Mascolo et al. 2013) have been utilized in coprecipitation method. The addition of different precipitants manipulates the pH of precursor's (Fe^{2+} and Fe^{3+}) solution to reach around 9–10 at which Fe_3O_4 NPs produced. The mechanism of Fe_3O_4 NPs formation during coprecipitation was not clearly understood. Recently, reaction pathways of magnetite NPs have been investigated based on the rate of addition of a reducing agent into precursor's mixture (Ahn et al. 2012). Upon fast addition, goethite (α-FeOOH) and ferrous hydroxide ($Fe(OH)_2$) are the key intermediates controlling phase transformation and growth of stable Fe_3O_4 NPs.

The magnetite NPs reveal a variety of applications due to their high saturation magnetization ($M_S^{bulk} \sim 92$ emu g^{-1}) (Nikiforov et al. 2013). The magnetic characteristics of Fe_3O_4 are size dependent and show superparamagnetic characteristics at room temperature when their size is < 25 nm (Khosroshahi and Tajabadi 2016). This phenomenon allows the suitability of SPIONs in various MRI applications. However, it is difficult to control the size and shape of Fe_3O_4 NPs during the synthesis as only kinetic factors are available to monitor the growth. To overcome this obstacle, various approaches were adopted such as the use of chelating agents and tight control over reaction parameters, i.e., temperature, pH, metal cation concentrations, stirring rate, and type of reducing agent. In addition, various surfactants can be added to the reaction mixture, where micelle control the size and shape of NPs in continuous phase (Willard et al. 2004). However, it is laborious work to remove surfactant from nanoparticle's surface entirely, which results in decreasing their superparamagnetic characteristics. Thus, controlling size and shape of SPIONs without using surfactant remain a challenging task.

Over the years, researchers investigated the effect of different reaction parameters on particle size of Fe_3O_4 NPs synthesized via coprecipitation protocol. The average crystallite size of magnetite NPs gradually decreased from 24.0 to 22.3 nm until 700 rpm and then contrarily increased to 25 nm until 900 rpm (Rahmawati et al. 2017). The effect of temperature (20, 70 °C) and NH_4OH concentration (0.9–2.1 M) was also studied on size and magnetic properties of Fe_3O_4 NPs (Tajabadi and Khosroshahi 2012). The role of pH has been investigated on structural, optical, and magnetic properties of Fe_3O_4 NPs. The complete coprecipitation of magnetite NPs occurred at high pH 10 (Wu et al. 2008; Rani and Varma 2015). It is challenging to synthesize pure magnetite phase with less concentration of OH^- ions efficiently.

The size of Fe_3O_4 NPs controlled between 8 and 50 nm by varying the amount of urea decomposition via adjusting the reaction time (Jiang et al. 2004). Furthermore, the role of reaction parameters on particle size has also been investigated during coprecipitation and the smallest particle size attained was 40.9 nm with a polydispersity of 0.194 (Sayar et al. 2006). The observed particle size was still higher than the critical diameter (D_p ~25 nm) for magnetite NPs to behave like superparamagnetic materials. It is hard to find a comprehensive published work which systematically focuses on the influence of all possible parameters on size, shape, and magnetic properties of magnetite NPs. In most of the reported studies, only one or two parameters are considered together, which may not be sufficient to fully understand the effects of interdependent optimum conditions for shape- and size-controlled coprecipitation of Fe_3O_4 NPs.

In the present work, we experimentally optimized a range of possible reaction parameters to obtain relatively smaller particle size (< 15 nm) and various shapes of SPIONs via chemical coprecipitation. We extensively investigated the role of stirring rate, temperature, reaction time, pH, and

type of reducing agent on nucleation, particle's growth, size, shape, and morphology of SPIONs via TEM. The synthesized SPIONs were further characterized by various material characterization techniques. Finally, T_2-relaxation measurements and relaxometry properties of synthesized SPIONs were investigated in harsh saline water to determine the possibility of these contrast agents for MRI of the oil reservoirs. The presented work describes the novelty in terms of synthesis of shape-controlled SPIONs under optimum conditions without using a surfactant and determination of relaxometric properties using a miniaturized revolutionary instrument, i.e., Acorn Area analyzer.

Experimental

Synthesis of SPIONs

SPIONs were prepared via chemical coprecipitation of Fe^{3+} and Fe^{2+} (2:1) using NH_4OH as a reducing agent. The mixing was performed by overhead Teflon stirrer in Ar atmosphere. A series of experiments (E1–E16, Table 1) were conducted to optimize the stirring rate, temperature, pH, and reaction time for synthesis of SPIONs. After optimizing the reaction parameters with NH_4OH, three experiments (E17–E19, Table 1) were further performed to study the effect of reducing agents (NH_4OH, KOH, and NaOH) on particle shape, size, and magnetic properties of SPIONs. The magnetite NPs synthesized by various reducing agents were labeled as MNP–NH_4OH, MNP–KOH, and MNP–NaOH, respectively. For each experiment, 0.5 mL of conc. HCl was mixed with 50 mL of deionized water to make it acidified (pH 1.5) and purged it with Ar gas for 15 min. Then, 0.6 M $FeCl_3.6H_2O$ and 0.3 M $FeCl_2{\cdot}4H_2O$ solutions were prepared in acidified water. The precursor's solutions were mixed and heated up to a certain temperature. Then, required amount of reducing agent be vigorously poured into the iron precursor's solution at a particular stirring rate. The color of solution changed to brownish black or black showing the NPs' growth. The reaction mixture was continuously heated and stirred for a particular time, and tetramethyl ammonium hydroxide (TMAH, 25 wt%) was added dropwise to stabilize the synthesized particles. The mixture was cool down to ambient temperature. The NPs were centrifuged at 15,000 rpm, washed with ethanol, and dried at 80 °C for 24 h. The schematic representation of SPIONs' formation under optimized reaction conditions is provided in Fig. 1. A detail of material characterization techniques and preparation of synthetic seawater (SW) is provided in ESI section.

T_2-relaxation measurements

To assess the feasibility of synthesized magnetite NPs as T_2-contrast agents, relaxation measurements were performed using a portable NMR-based Acorn Area particle analyzer (Xigo Nanotools, USA). For each measurement, 1 mL

Table 1 Various experimental conditions for synthesis of magnetite NPs

Experiment #	Stirring rate (rpm)	Temperature (°C)	Reaction time (h)	pH	Precipitating agent	Observed parameter
E1	100	80	1.0	9.0	NH_4OH	Effect of stirring rate
E2	300	80	1.0	9.0	NH_4OH	
E3	500	80	1.0	9.0	NH_4OH	
E4	700	80	1.0	9.0	NH_4OH	
E5	500	20	1.0	9.0	NH_4OH	Effect of temperature
E6	500	40	1.0	9.0	NH_4OH	
E7	500	60	1.0	9.0	NH_4OH	
E8	500	80	1.0	9.0	NH_4OH	
E9	500	80	0.5	9.0	NH_4OH	Effect of reaction time
E10	500	80	1.0	9.0	NH_4OH	
E11	500	80	2.0	9.0	NH_4OH	
E12	500	80	4.0	9.0	NH_4OH	
E13	500	80	1.0	4.5	NH_4OH	Effect of pH
E14	500	80	1.0	6.0	NH_4OH	
E15	500	80	1.0	7.5	NH_4OH	
E16	500	80	1.0	9.0	NH_4OH	
E17	500	80	1.0	9.0	NH_4OH	Effect of precipitating agent
E18	500	80	1.0	9.0	KOH	
E19	500	80	1.0	9.0	NaOH	

The molar ratio Fe^{3+}/Fe^{2+} (2:1) in all these experiments

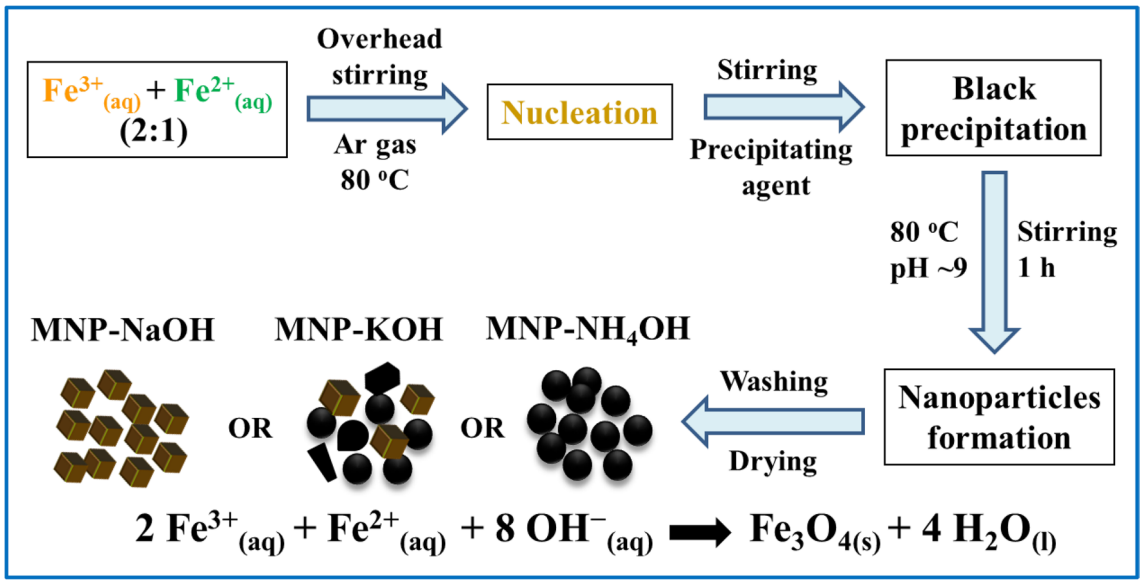

Fig. 1 Schematic representation of SPIONs formation during chemical coprecipitation

aqueous dispersion of magnetite NPs, prepared in SW, was kept in NMR sample tube. A standard pulse sequence, i.e., Carr–Purcell–Meiboom–Gill (CPMG), was applied to measure T_2-decay curve (Coates et al. 1999). All the experimental parameters such as tau (τ) value, recycle delay, NMR filed strength, resonating frequency, and number of scans are provided in our recent research work (Ali et al. 2018). T_2-relaxation curves versus various concentrations of magnetite NPs were recorded, and each measurement was repeated three times to attain the average T_2 value, which help to determine the contrasting ability in terms of r_2 value.

Results and discussion

A critical optimization of reaction parameters was performed to control the size, shape, and superparamagnetic characteristics of the synthesized NPs. The effect of various parameters such as (i) stirring rate, (ii) temperature, (iii) reaction time, and (iv) pH was comprehensively investigated via TEM. A detailed discussion of these parameters on particle's growth, size, and morphology is provided in ESI section along with their corresponding TEM images (Figs. S1–S4). After optimization of all the reaction conditions, the effect of various reducing agents on size and shape of SPIONs was examined. The synthesized MNP–NH_4OH, MNP–KOH, and MNP–NaOH nanomaterials were further characterized and their chemical stability was monitored in SW. Finally, T_2-relaxation measurements and relaxometry properties of SPIONs were investigated in SW for potential MRI application.

Role of reducing agents on shape of SPIONs

The reducing agents have a significant effect on size, shape, and magnetic properties of magnetite NPs. The saturation magnetization of magnetite NPs also increased as the strength of reducing agent decreased as follows (Gribanov et al. 1990): KOH > NaOH > NH_4OH. Based on the preliminary studies, the effect of reducing agents, i.e., NH_4OH, KOH, and NaOH on the synthesis of SPIONs was investigated. Rest of the optimized parameters, i.e., stirring rate ~ 500 rpm, temperature ~ 80 °C, reaction time ~ 1.0 h, and pH 9.0, were kept constant (E17–E19, Table 1). The correspondent (a–c) TEM images and (d–f) histograms are provided in Fig. 2. The different shapes of magnetite NPs observed by various reducing agents indicate that their strength plays a vital role in controlling the growth rate of crystal facets in different directions. The spherical-shaped NPs were mainly prepared with NH_4OH having average particle diameter ~ 9.1 ± 1.5 nm (Fig. 2a). The spherical shape was predominantly formed due to its least surface free-energy compared to other shapes (Kim et al. 2003). However, KOH gives a mixture of spherical- (~ 9.4 ± 1.9 nm) and irregular (~ 18.7 ± 2.5 nm)-shaped NPs (Fig. 2b). Owing to the highest strength of KOH, the faster growth rate of crystal facets observed in various direction. Moreover, NaOH mainly produces cubic-shaped magnetite NPs having average size ~ 11.7 ± 1.8 nm (Fig. 2c). The cubic shape of magnetite NPs was dominantly formed due to the faster crystal growth along (1 1 1) direction as compared to (1 0 0) plane (Yang et al. 2011). The comparison indicates that the smaller spherical- and cubic-shaped NPs were achieved using NH_4OH and NaOH, respectively, which are

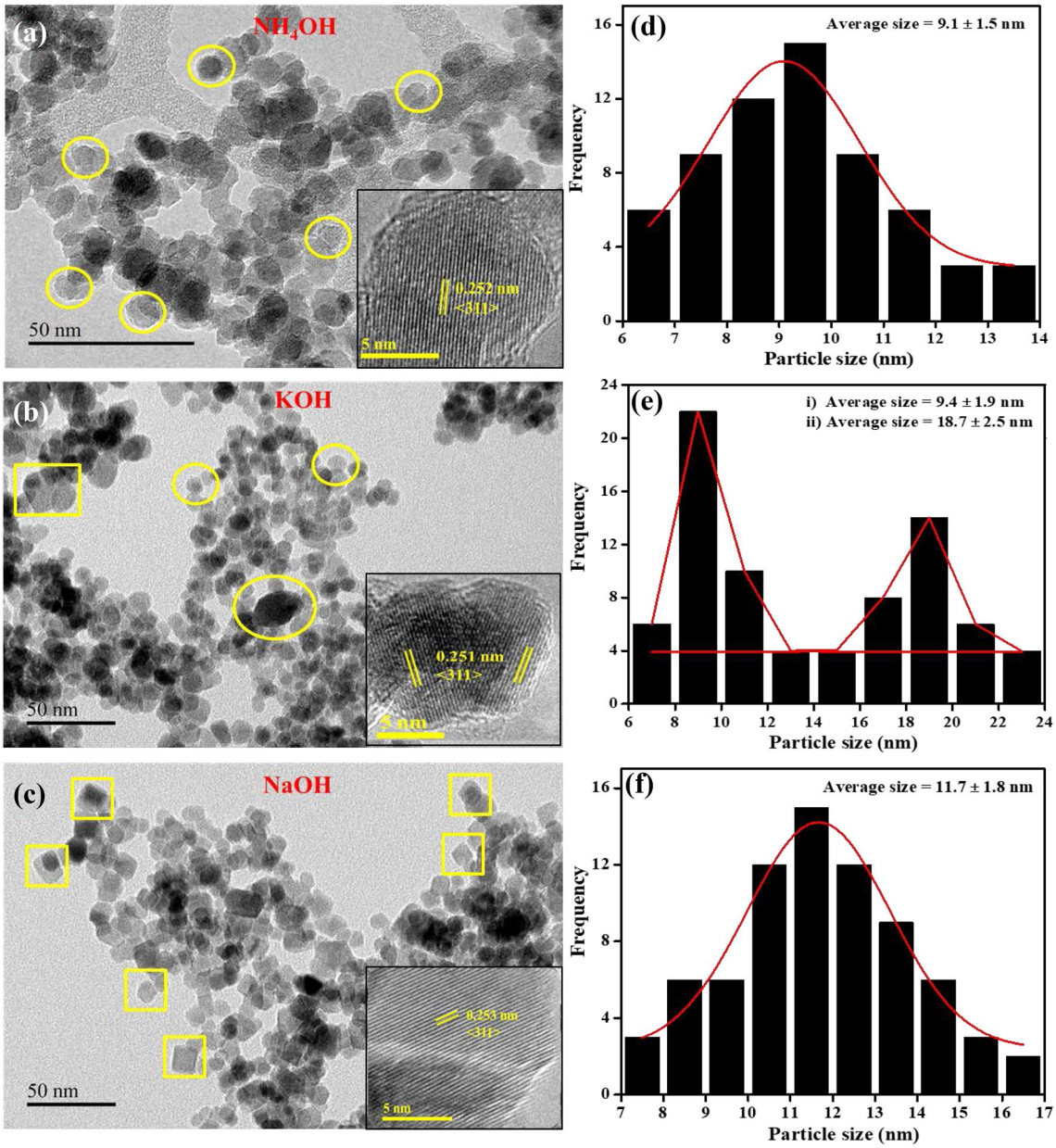

Fig. 2 **a–c** TEM images (insets: HRTEM images), and **d–f** histograms of samples (S17–S19) synthesized via NH_4OH, KOH, and NaOH, respectively

much lower than the reported size (~40 nm) of magnetite NPs under optimized conditions (Daou et al. 2006; Sayar et al. 2006). The crystal structure of magnetite NPs was further investigated via HRTEM as presented in the insets of Fig. 2a–c. The observed separation of lattice fringes matches well with the reported *d*-spacing value of 0.253 nm, which correspond to (3 1 1) crystal plane of magnetite structure.

The magnetic NPs show superparamagnetic behavior below the critical size (D_p). The approximate value of D_p can be calculated for spherical-shaped magnetite NPs using Eq. 2 (Khosroshahi and Tajabadi 2016):

$$V_p = k_b T / K, \tag{2}$$

where V_p is volume of spherical-shaped NPs, k_b denotes Boltzmann constant, and T is absolute temperature. The magnetic anisotropy constant (K) is temperature dependent, and its value is 1.35×10^4 J m^{-3} at 300 K for Fe_3O_4 NPs (Yoon 2011). From the above equation, the estimated D_p value for superparamagnetic behavior of magnetite NPs is ~25 nm. Our TEM results indicate that as-synthesized MNP–NH_4OH, MNP–KOH, and MNP–NaOH NPs have sizes < 25 nm which affirm their superparamagnetic

behavior. The comparative study confirms that controlling reaction parameters and selectively choosing reducing agents during coprecipitation, we can selectively design SPIONs of the desired size and shape for advanced applications.

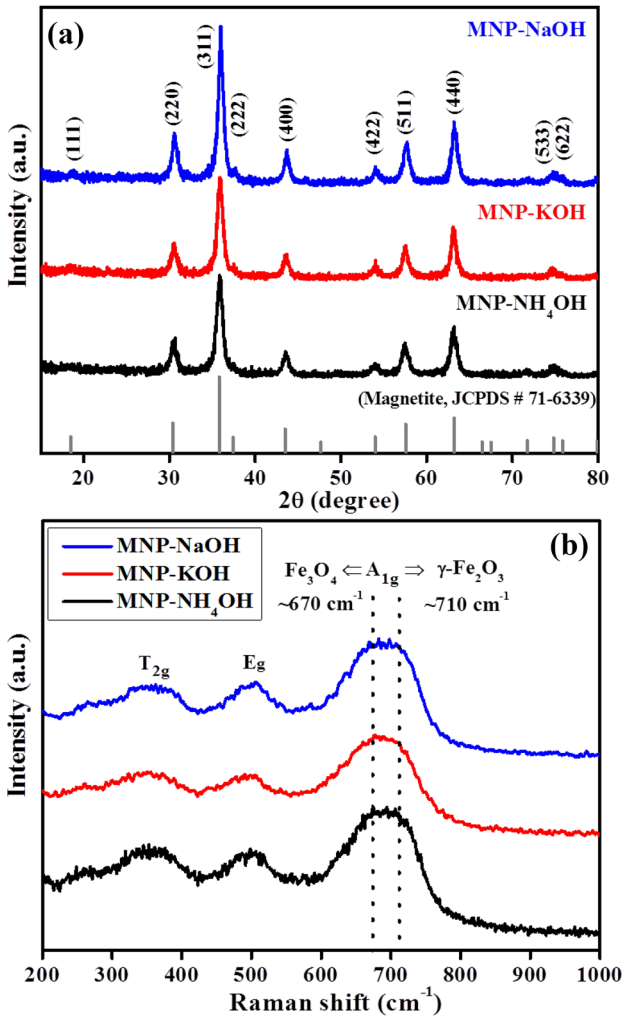

Fig. 3 **a** XRD and **b** Raman spectra of SPIONs synthesized using NH_4OH, KOH, and NaOH

Structural properties and phase analyses

The phase, crystal structure, and purity of SPIONs were investigated via X-rays diffraction (XRD) analysis. Figure 3a displays the diffraction patterns of SPIONs prepared using three different reducing agents (NH_4OH, KOH, and NaOH). The observed diffractograms match-well with standard pattern (JCPDS card-71-6339) suggesting the formation of magnetite phase (Sun et al. 2012). The five characteristics peaks appeared at $2\theta = 30.50°$, 35.87°, 43.65°, 57.54°, and 63.28° assigned to (2 2 0), (3 1 1), (4 0 0), (5 1 1), and (4 4 0) crystalline planes, respectively. Moreover, Fe_3O_4 NPs exhibit a cubic inverse spinel structure (*Fd-3m* space group) (Cornell and Schwertmann 2003). The average crystallite size of magnetite NPs was evaluated from (3 1 1) diffraction plane using Debye–Scherrer equation (Ali et al. 2017b, a). It was found to be ~ 11.2, ~ 12.0 and ~ 13.9 nm for MNP–NH_4OH, MNP–KOH, and MNP–NaOH, respectively (Table 2). The unit cell parameters (a) and cell volume (V) for SPIONs are also provided in Table 2. The comparison shows estimated values of average crystallite sizes of SPIONs are consistent with unit cell parameters. The average crystallite size, cell parameters, and cell volume increase in the following order: NH_4OH < KOH < NaOH. This order indicates that the reducing agent plays a pivotal role in controlling the dimensions and crystal structure of particles. Moreover, calculated values of crystallite sizes are also agree-well with particles sizes estimated from TEM images. It is well-established that γ-Fe_2O_3 and Fe_3O_4 reveal similar XRD profiles (Zhang et al. 2013). Therefore, SPIONs were further characterized by surface-enhanced Raman scattering (SERS) and X-ray photoelectron spectroscopy (XPS) techniques, which exclusively identify the presence of γ-Fe_2O_3 and Fe_3O_4 phases.

The phases of iron oxides NPs were elucidated via SERS technique by detecting their Raman active phonon modes. Figure 3b shows Raman spectra of as-synthesized powder materials. The observed Raman spectra are similar and show the broad bands with low signal-to-noise ratio. The broad characteristic band in each spectrum having two shoulders observed around ~ 670 cm^{-1} and ~ 705 cm^{-1} corresponded to phonon modes (A_{1g}) of Fe_3O_4 and γ-Fe_2O_3, respectively

Table 2 Summary of various parameters evaluated from XRD, Raman, TEM, and BET results of SPIONs

SPIONs	XRD				Raman	TEM		BET	
Sample	Crystallite size (nm)	Unit cell parameter (Å)	Unit cell volume (Å^3)	Phase composition	Surface composition	Shape	Size (nm)	Specific surface area ($m^2\ g^{-1}$)	Diameter D_{BET} (nm)
MNP–NH_4OH	11.2	8.299	571.7	Fe_3O_4	Fe_3O_4 + γ-Fe_2O_3	Spherical	9.1 ± 1.5	101.4	11.4
MNP–KOH	12.0	8.303	572.4	Fe_3O_4	Fe_3O_4 + γ-Fe_2O_3	Spherical Irregular	9.4 ± 1.9 18.7 ± 2.5	81.5	14.2
MNP–NaOH	13.9	8.326	577.2	Fe_3O_4	Fe_3O_4 + γ-Fe_2O_3	Cubic	11.7 ± 1.8	75.3	15.4

(Shebanova and Lazor 2003; Jubb and Allen 2010). This indicates the coexistence of Fe_3O_4 with γ-Fe_2O_3 phase at the surface due to overoxidation of NPs surfaces. Moreover, two broad bands having center near ~ 505 cm^{-1} and 340 cm^{-1} associated with E_g and T_{2g} modes of the admixture (Fe_3O_4, γ-Fe_2O_3), respectively (Zhang et al. 2013). A similar phenomenon, i.e., the coexistence of Fe_3O_4 with γ-Fe_2O_3 at the outermost surface of magnetite NPs, is reported in the literature (Kolen'ko et al. 2014). This is due to the oxidation–reduction phenomenon of magnetite NPs surfaces under basic conditions. Another reason is described and supported by the mechanism of mixing domain at the molecular level during synthesis process (Wang and Shaw 2014).

X-rays photoelectron spectroscopy technique was further utilized to determine the oxidation states of constituent elements present in SPIONs. Figure 4a, b shows Fe 2*p* spectra of MNP–NH_4OH, MNP–KOH, and MNP–NaOH before and after 50 s etching. XPS profiles of Fe in Fig. 4a exhibit two separate peaks appeared at binding energies of 711.0 and 724.5 eV (spin–orbit splitting, $\Delta = 13.5$ eV) assigned to Fe $2p_{3/2}$ and Fe $2p_{1/2}$ of γ-Fe_2O_3 phase. Furthermore, the appearance of satellite peaks at 719.0 eV in Fe profiles (encircled in Fig. 4a) confirms the presence of γ-Fe_2O_3 phase. It is well-established that Fe $2p_{3/2}$ spectrum does not shows satellite peak for Fe_3O_4 (Wang et al. 2014; Liu et al. 2015). After 50 s of etching (Fig. 4b), Fe $2p_{3/2}$ and Fe $2p_{1/2}$ peaks shifted to the binding energies of 710.6 and 724.1 eV ($\Delta = 13.5$ eV) with no satellite peak, which confirms the presence of Fe_3O_4 phase in the bulk material. The observed spectra match-well with the standard Fe_3O_4 sample (Yamashita and Hayes 2008).

The specific surface area and porosity of SPIONs synthesized by NH_4OH, KOH, and NaOH were estimated from the N_2 adsorption–desorption isotherms. The isotherms were attained by plotting the relative pressure (P/P_o) against volume adsorbed ($cm^3\ g^{-1}$ at STP), as provided in Fig. 5a. Brunauer, Emmett, and Teller (BET) surface area of MNP–NH_4OH, MNP–KOH, and MNP–NaOH was found to be 101.4, 81.5, and 75.3 $m^2\ g^{-1}$, respectively. The average diameter of NPs (D_{BET}) was also estimated from BET surface area (Mascolo et al. 2013), and the values were found to be 11.4, 14.2, and 15.4 nm, respectively (Table 2). The adsorption isotherms indicate that NPs' sizes of synthesized materials are in good agreement with their TEM results. The pore sizes (20.0, 13.9, and 12.4 nm) and pore volumes (0.47, 0.28, and 0.24 $cm^3\ g^{-1}$) were also evaluated from Barrett–Joyner–Halenda (BJH) adsorption isotherms (Fig. 5b), respectively. Furthermore, BET and BJH results suggest that synthesized SPIONs are slightly mesoporous.

Chemical stability and magnetic properties of SPIONs

The magnetic character and chemical stability of magnetite NPs in the harsh saline environment have vital role for their ultimate well-logging application. Therefore, the magnetic properties and stability of SPIONs were examined in SW having salinity 36.03 g L^{-1} and pH 8.0. For each test, 10.0 mg of nano-powder was dispersed in 2.5 mL of deionized water by ultrasonication for 30 min. Figure 6a–c demonstrates the stable dispersion of (a) MNP–NH_4OH, (b) MNP–KOH, and (c) MNP–NaOH in SW environment in the absence of an applied magnetic field. It was observed that synthesized Fe_3O_4 NPs possess hydrophilic characteristics due to the presence of –OH groups on their surface due to the hydroxylation phenomenon during coprecipitation (Shaterian and Aghakhanizadeh 2013). After applying a magnetic field, SPIONs showed magnetic behavior

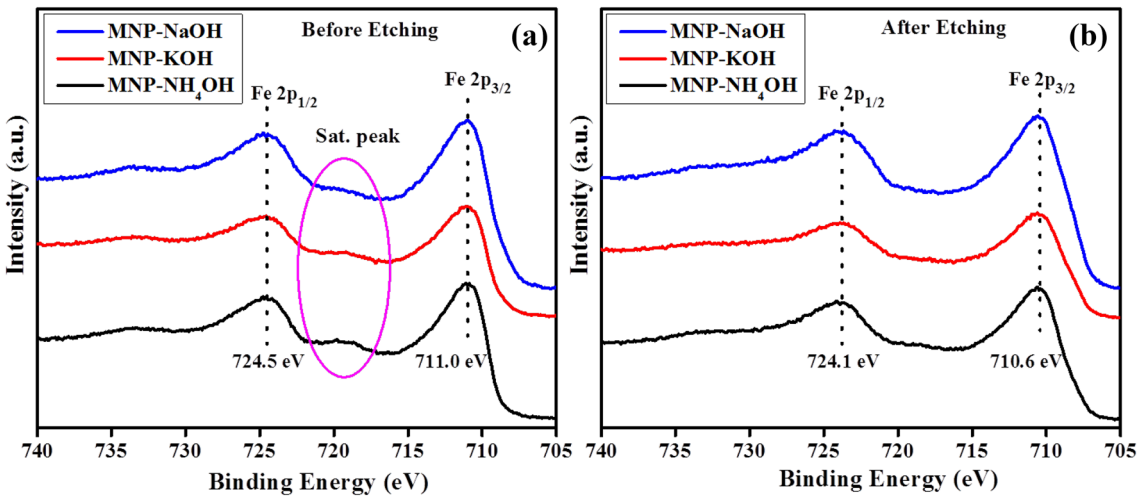

Fig. 4 XPS (Fe 2*p*) profiles of SPIONs (**a**) before and (**b**) after 50 s etching

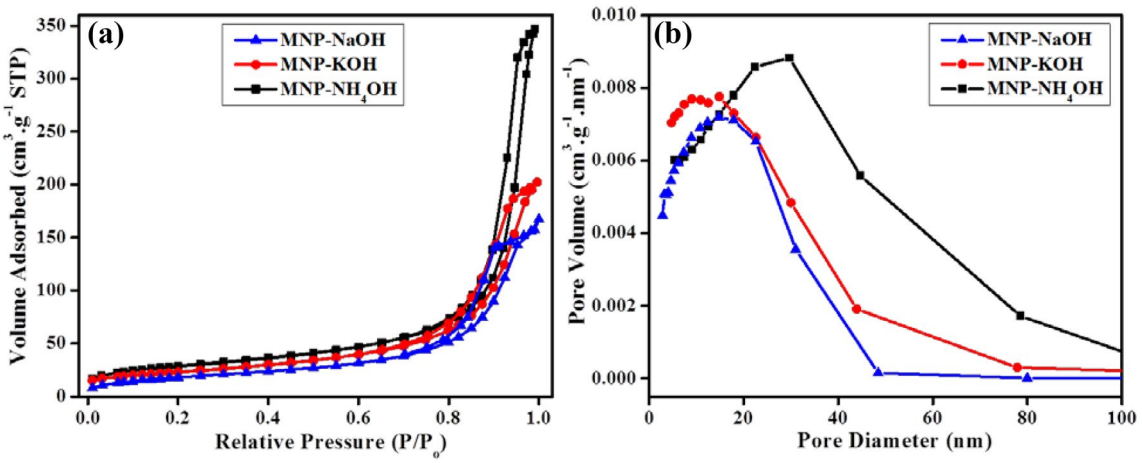

Fig. 5 **a** N_2 adsorption–desorption isotherms and **b** pore size distribution of SPIONs

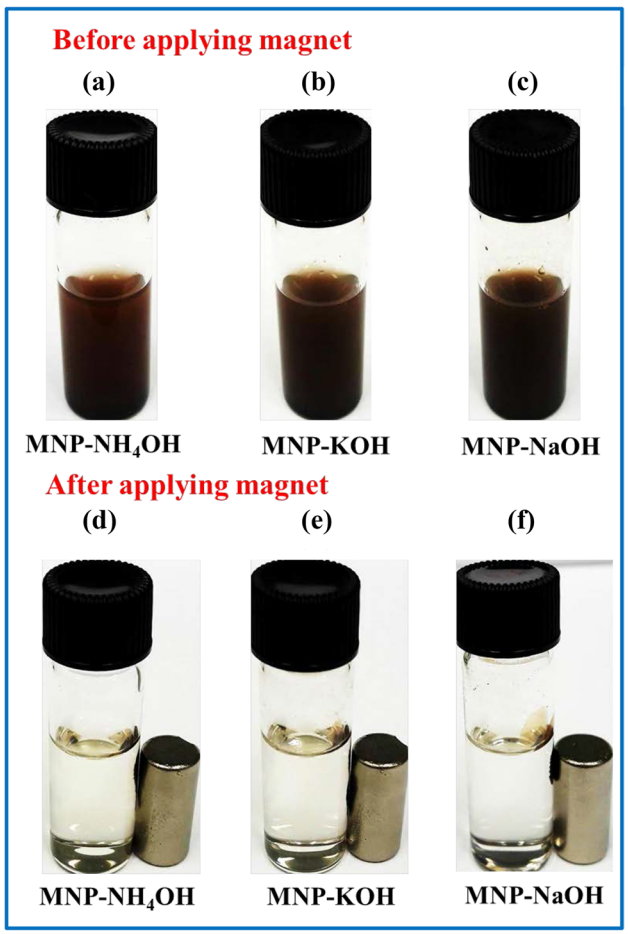

Fig. 6 Magnetic behavior of MNP–NH_4OH, MNP–KOH, and MNP–NaOH samples in ASW (**a**–**c**) before and (**d**–**f**) after applying external magnetic field

and strongly attracted to the magnet, as demonstrated in Fig. 6d–f. Moreover, SPIONs persisted chemical stability in the saline environment for 1 week, because the magnetite nanoparticles are pH dependent and their surface gets oxidized in aqueous medium when pH < 7 (Sayar et al. 2006). Owing to their chemical stability and magnetic behavior, these NPs can be utilized as T_2-contrast agents for MRI of fluids present within the oil-bearing rocks.

Relaxometry studies of SPIONs

NMR T_2-relaxation measurements were carried out for various concentrations of as-synthesized SPIONs, and relaxivity properties (r_2 values) were assessed for targeted oil reservoir applications. For each synthesized nanomaterial, six various concentrations such as 0.001, 0.005, 0.010, 0.025, 0.050, and 0.100 mM having Fe concentrations, i.e., 0.03, 0.015, 0.030, 0.075, 0.150, and 0.300 mM were produced to measure relaxometry characteristics of SPIONs in SW. T_2-relaxation signals as well as T_2 values of (a) MNP–NH_4OH, (b) MNP–KOH, and (c) MNP–NaOH having various Fe (mM) are presented in Fig. 7. It was observed that increase in concentration of magnetite NPs enhanced the T_2-relaxation signal. This phenomenon can be explained by NMR relaxation which occurred owing to the exchange in energy of neighboring protons in SW. The magnetic material induces field inhomogeneity and de-phase the magnetic moments of protons in the presence of an applied magnetic field, which increased the surface relaxation. The enhanced surface relaxation values, i.e., 78, 157, and 110 ms against Fe (0.300 mM) concentration observed for MNP–NH_4OH, MNP–KOH, and MNP–NaOH, respectively. The comparison indicates that MNP–NH_4OH exhibits the better relaxation due to the smaller size and higher surface area of NPs. The incorporation of SPIONs in SW enhanced the surface

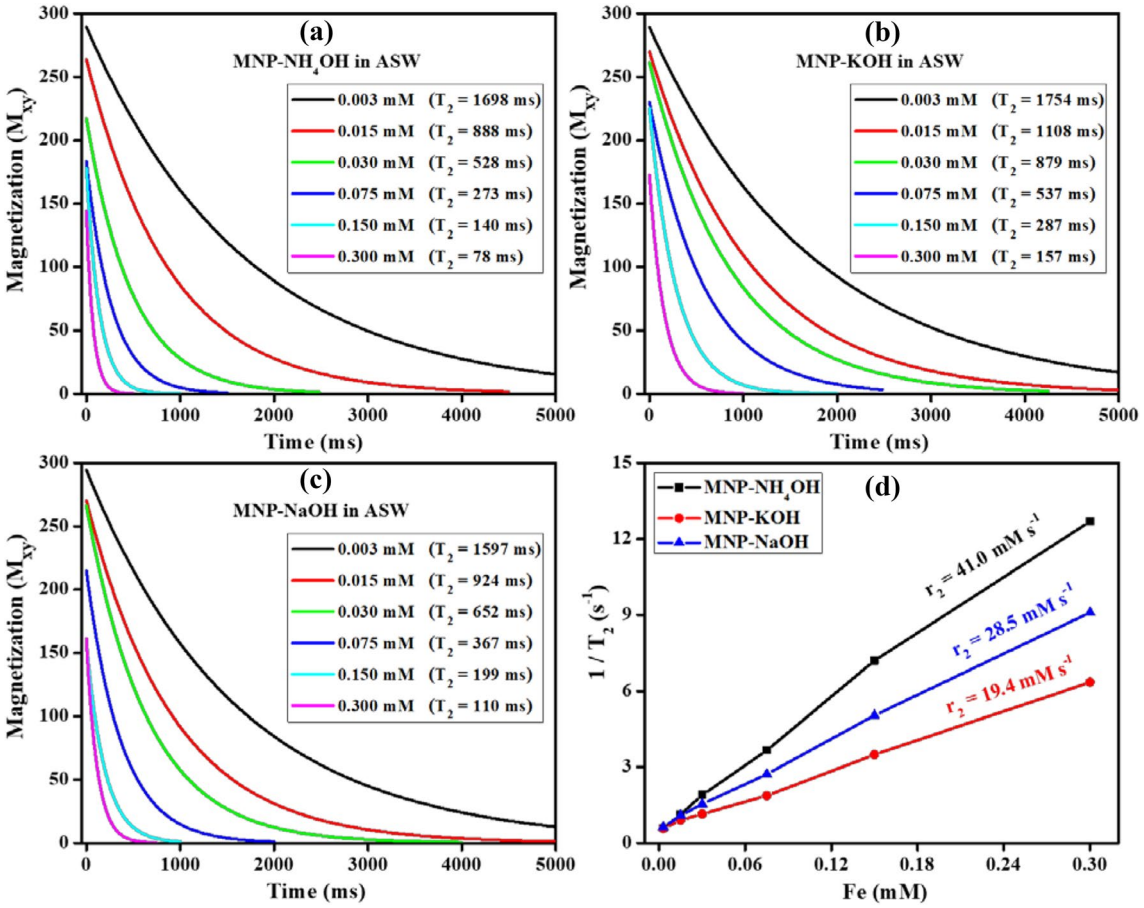

Fig. 7 **a**–**c** T_2-relaxation signals for various Fe (mM) concentrations of MNP–NH_4OH, MNP–KOH, and MNP–NaOH, respectively. **d** Inverse of relaxation time ($1/T_2$) against various Fe (mM) concentrations of magnetite NPs

relaxation of water protons, which enable the NMR well-logging at higher speed. Therefore, MNP–NH_4OH can be promising NMR T_2-contrast agent for well-logging application.

To estimate the relaxometry properties in terms of transverse (r_2) relaxivity, the inverse of relaxation time ($1/T_2$, s^{-1}) values were plotted against various Fe (mM) concentrations (Fig. 7d) by the following equation (3):

$$1/T_2 = 1/T_2^{o} + r_2[\mathrm{Fe}], \tag{3}$$

where T_2 is the relaxation time of NPs dispersion, T_2^{o} is the relaxation time of SW, and r_2 is the transverse relaxivity. The r_2 values were found to be 41.0, 28.5, and 19.4 mM^{-1} s^{-1} for MNP–NH_4OH, MNP–KOH, and MNP–NaOH, respectively. The comparison shows that the r_2 values for MNP–NH_4OH (spherical) and MNP–NaOH (cubic) are 2.11 and 1.47 times higher than MNP–KOH (irregular), respectively. The spherical- and cubic-shaped SPIONs showed higher relaxivity owing to their smaller size, better shape homogeneity and higher surface area as compared to the irregular-shaped SPIONs. Moreover, the observed r_2 value for MNP–NH_4OH (41.0 mM^{-1} s^{-1}) is ~7.8 times greater than commercial contrast agent (Gd-DTPA, $r_2 = 5.3$ mM^{-1} s^{-1}) and found competitive with ultrasmall magnetite NPs ($r_2 = 35.1$ mM^{-1} s^{-1}) (Li et al. 2012). The enhanced surface relaxation and observed relaxivity properties indicate that the synthesized SPIONs can be efficiently utilized as T_2-contrast agents for MRI applications.

Conclusions

Shape- and size-controlled SPIONs have been successfully prepared via chemical coprecipitation protocol without using surfactant. The optimum reaction conditions for the synthesis were found to be (i) stirring rate ~ 500 rpm; (ii) temperature ~ 80 °C; (iii) reaction time ~ 1.0 h; and (iv) pH 9.0. Among all the studied parameters, the effect of pH, temperature, and reducing agent was significant on the size, shape, and magnetic properties of SPIONs. Our straightforward approach to synthesize SPIONs of spherical- and cubic-shaped having size (9.1 ± 1.5 nm) and (11.7 ± 1.8 nm) just by changing the reducing agent, i.e., NH_4OH and NaOH,

respectively, is more advantageous as compared to some previously reported thermal decomposition strategies (Kim et al. 2008a; Yang et al. 2008). The spherical shape was predominantly formed due to its least surface free-energy compared to other shapes, while cubic shape was primarily observed owing to the faster crystal growth along (1 1 1) direction as compared to (1 0 0) plane. The magnetite phase of SPIONs was confirmed XRD and XPS analyses. The synthesized SPIONs were found stable in saline water. The enhanced NMR T_2-relaxation and excellent transverse relaxivity properties of SPIONs in SW exhibit their potential utilization as T_2-contrast agents for MRI of oil reservoirs. Future work will be focused on the utility of these SPIONs in brine/oil saturated carbonate and sandstone rock cores for NMR signals separation and their quantification.

Acknowledgements The authors are thankful to the "Center of Research Excellence in Nanotechnology (CENT) at King Fahd University of Petroleum and Minerals (KFUPM) in the Kingdom of Saudi Arabia." for providing the research facilities.

Compliance with ethical standards

Conflict of interest On behalf of all authors, the corresponding author states that there is no conflict of interest.

References

Abbas M, Parvatheeswara Rao B, Nazrul Islam M et al (2014) Highly stable-silica encapsulating magnetite nanoparticles (Fe_3O_4/SiO_2) synthesized using single surfactantless-polyol process. Ceram Int 40:1379–1385. https://doi.org/10.1016/j.ceramint.2013.07.019

Ahn T, Kim JH, Yang H-M et al (2012) Formation Pathways of magnetite nanoparticles by coprecipitation method. J Phys Chem C 116:6069–6076. https://doi.org/10.1021/jp211843g

Ali S, Khan I, Khan SA et al (2017a) Plasmon aided ($BiVO_4$)x–(TiO_2)1–x ternary nanocomposites for efficient solar water splitting. Sol Energy 155:770–780. https://doi.org/10.1016/J.SOLENER.2017.07.031

Ali S, Khan SA, Khan I et al (2017b) Surfactant-free synthesis of ellipsoidal and spherical shaped TiO 2 nanoparticles and their comparative photocatalytic studies. J Environ Chem Eng 5:3956–3962. https://doi.org/10.1016/j.jece.2017.07.066

Ali S, Khan SA, Eastoe J et al (2018) Synthesis, characterization, and relaxometry studies of hydrophilic and hydrophobic superparamagnetic Fe_3O_4 nanoparticles for oil reservoir applications. Colloids Surf A Physicochem Eng Asp 543:133–143. https://doi.org/10.1016/J.COLSURFA.2018.02.002

Cha J, Cui P, Lee J-K (2010) A simple method to synthesize multifunctional silica nanocomposites, NPs@SiO_2, using polyvinylpyrrolidone (PVP) as a mediator. J Mater Chem 20:5533. https://doi.org/10.1039/b924702e

Chi L, Cheng K, Heidari Z (2016) Improved assessment of interconnected porosity in multiple-porosity rocks by use of nanoparticle contrast agents and nuclear-magnetic-resonance relaxation measurements. SPE Reserv Eval Eng 19:095–107. https://doi.org/10.2118/170792-PA

Coates G, Xiao L, Prammer M (1999) NMR logging: principles and applications. Haliburton Energy Services, Houston

Cornell RM, Schwertmann U (2003) The iron oxides. Wiley-VCH Verlag GmbH & Co. KGaA, Weinheim

Daou TJ, Pourroy G, Begin-Colin S et al (2006) Hydrothermal synthesis of monodisperse magnetite nanoparticles. Chem Mater 18:4399–4404

Ditsch A, Lindenmann S, Laibinis PE et al (2005) High-gradient magnetic separation of magnetic nanoclusters. Ind Eng Chem Res 44:6824–6836

Du X, Wang C, Chen M et al (2009) Electrochemical performances of nanoparticle Fe_3O_4/activated carbon supercapacitor using KOH electrolyte solution. J Phys Chem C 113:2643–2646

Gao Z, Ma T, Zhao E et al (2016) Small is smarter: nano MRI contrast agents—advantages and recent achievements. Small 12:556–576. https://doi.org/10.1002/smll.201502309

Gawande MB, Branco PS, Varma RS (2013) Nano-magnetite (Fe_3O_4) as a support for recyclable catalysts in the development of sustainable methodologies. Chem Soc Rev 42:3371–3393. https://doi.org/10.1039/C3CS35480F

Gribanov NM, Bibik EE, Buzunov OV, Naumov VN (1990) Physicochemical regularities of obtaining highly dispersed magnetite by the method of chemical condensation. J Magn Magn Mater 85:7–10

Jiang W, Yang HCC, Yang SYY et al (2004) Preparation and properties of superparamagnetic nanoparticles with narrow size distribution and biocompatible. J Magn Magn Mater 283:210–214. https://doi.org/10.1016/j.jmmm.2004.05.022

Jiang QL, Zheng SW, Hong RY et al (2014) Folic acid-conjugated Fe_3O_4 magnetic nanoparticles for hyperthermia and MRI in vitro and in vivo. Appl Surf Sci 307:224–233. https://doi.org/10.1016/j.apsusc.2014.04.018

Jubb AM, Allen HC (2010) Vibrational spectroscopic characterization of hematite, maghemite, and magnetite thin films produced by vapor deposition. ACS Appl Mater Interfaces 2:2804–2812

Khan US, Rahim A, Khan N et al (2017) Aging study of the powdered magnetite nanoparticles. Mater Chem Phys 189:86–89. https://doi.org/10.1016/J.MATCHEMPHYS.2016.12.047

Khosroshahi ME, Tajabadi M (2016) Characterization and cellular fluorescence microscopy of superparamagnetic nanoparticles functionalized with third generation nanomolecular dendrimers: in-vitro cytotoxicity and uptake study. J Nanomater Mol Nanotechnol 5:1–11

Kim DK, Mikhaylova M, Zhang Y, Muhammed M (2003) Protective coating of superparamagnetic iron oxide nanoparticles. Chem Mater 15:1617–1627

Kim D, Lee N, Park M et al (2008a) Synthesis of uniform ferrimagnetic magnetite nanocubes. J Am Chem Soc 131:454–455

Kim J, Lee JE, Lee SH et al (2008b) Designed fabrication of a multifunctional polymer nanomedical platform for simultaneous cancer-targeted imaging and magnetically guided drug delivery. Adv Mater 20:478–483

Kolen'ko YV, Bañobre-López M, Rodríguez-Abreu C et al (2014) Large-scale synthesis of colloidal Fe_3O_4 nanoparticles exhibiting high heating efficiency in magnetic hyperthermia. J Phys Chem C 118:8691–8701

Li Z, Yi PW, Sun Q et al (2012) Ultrasmall water-soluble and biocompatible magnetic iron oxide nanoparticles as positive and negative dual contrast agents. Adv Funct Mater 22:2387–2393. https://doi.org/10.1002/adfm.201103123

Liu F, Cao PJ, Zhang HR et al (2005) Novel nanopyramid arrays of magnetite. Adv Mater 17:1893–1897

Liu XD, Chen H, Liu SS et al (2015) Hydrothermal synthesis of superparamagnetic Fe_3O_4 nanoparticles with ionic liquids as stabilizer. Mater Res Bull 62:217–221. https://doi.org/10.1016/j.materresbull.2014.11.022

Maeng JH, Lee D-H, Jung KH et al (2010) Multifunctional doxorubicin loaded superparamagnetic iron oxide nanoparticles for

chemotherapy and magnetic resonance imaging in liver cancer. Biomaterials 31:4995–5006
Mascolo MC, Pei Y, Ring TA (2013) Room temperature co-precipitation synthesis of magnetite nanoparticles in a large pH window with different bases. Materials (Basel) 6:5549–5567. https://doi.org/10.3390/ma6125549
Mitra S, Poizot P, Finke A, Tarascon J (2006) Growth and electrochemical characterization versus lithium of Fe_3O_4 electrodes made by electrodeposition. Adv Funct Mater 16:2281–2287
Moeser GD, Roach KA, Green WH et al (2002) Water-based magnetic fluids as extractants for synthetic organic compounds. Ind Eng Chem Res 41:4739–4749
Nikiforov VN, Koksharov YA, Polyakov SN et al (2013) Magnetism and Verwey transition in magnetite nanoparticles in thin polymer film. J Alloys Compd 569:58–61. https://doi.org/10.1016/j.jallcom.2013.02.059
Odagawa A, Katoh Y, Kanzawa Y et al (2007) Electroforming and resistance-switching mechanism in a magnetite thin film. Appl Phys Lett 91:133503
Okoli C, Sanchez-Dominguez M, Boutonnet M et al (2012) Comparison and functionalization study of microemulsion-prepared magnetic iron oxide nanoparticles. Langmuir 28:8479–8485
Patsula V, Kosinová L, Lovrić M et al (2016) Superparamagnetic Fe_3O_4 nanoparticles: synthesis by thermal decomposition of iron(III) glucuronate and application in magnetic resonance imaging. ACS Appl Mater Interfaces 8:7238–7247. https://doi.org/10.1021/acsami.5b12720
Rahmawati R, Permana MG, Harison B et al (2017) Optimization of frequency and stirring rate for synthesis of magnetite (Fe_3O_4) nanoparticles by using coprecipitation-ultrasonic irradiation methods. Proc Eng 170:55–59
Rani S, Varma GD (2015) Superparamagnetism and metamagnetic transition in Fe_3O_4 nanoparticles synthesized via co-precipitation method at different pH. Phys B Condens Matter 472:66–77
Roth H-C, Schwaminger SP, Schindler M et al (2015) Influencing factors in the CO-precipitation process of superparamagnetic iron oxide nano particles: a model based study. J Magn Magn Mater 377:81–89
Sayar F, Güen G, Pişkin E (2006) Magnetically loaded poly(methyl methacrylate-co-acrylic acid) nano-particles. Colloid Polym Sci 284:965–978. https://doi.org/10.1007/s00396-005-1383-5
Shaterian HR, Aghakhanizadeh M (2013) Aminopropyl coated on magnetic Fe_3O_4 and SBA-15 nanoparticles catalyzed mild preparation of chromeno [2, 3-d] pyrimidines under ambient and solvent-free conditions. Catal Sci Technol 3:425–428
Shebanova ON, Lazor P (2003) Raman spectroscopic study of magnetite ($FeFe_2O_4$): a new assignment for the vibrational spectrum. J Solid State Chem 174:424–430. https://doi.org/10.1016/S0022-4596(03)00294-9
Shi D, Cho HS, Chen Y et al (2009) Fluorescent polystyrene—Fe_3O_4 composite nanospheres for in vivo imaging and hyperthermia. Adv Mater 21:2170–2173
Sun H, Chen B, Jiao X et al (2012) Solvothermal synthesis of tunable electroactive magnetite nanorods by controlling the side reaction. J Phys Chem C 116:5476–5481
Tajabadi M, Khosroshahi ME (2012) Effect of alkaline media concentration and modification of temperature on magnetite synthesis method using $FeSO_4/NH_4OH$. Int J Chem Eng Appl 3:206–210. https://doi.org/10.7763/IJCEA.2012.V3.187
Unni M, Uhl AM, Savliwala S et al (2017) Thermal decomposition synthesis of iron oxide nanoparticles with diminished magnetic dead layer by controlled addition of oxygen. ACS Nano 11:2284–2303
Wang C, Shaw LL (2014) On synthesis of Fe_2SiO_4/SiO_2 and Fe_2O_3/SiO_2 composites through sol–gel and solid-state reactions. J Sol Gel Sci Technol 72:602–614. https://doi.org/10.1007/s10971-014-3483-5
Wang L, Neoh K-G, Kang E-T et al (2010) Biodegradable magnetic-fluorescent magnetite/poly(dl-lactic acid-co-α,β-malic acid) composite nanoparticles for stem cell labeling. Biomaterials 31:3502–3511. https://doi.org/10.1016/j.biomaterials.2010.01.081
Wang G, Zhang X, Skallberg A et al (2014) One-step synthesis of water-dispersible ultra-small Fe_3O_4 nanoparticles as contrast agents for T1 and T2 magnetic resonance imaging. Nanoscale 6:2953–2963. https://doi.org/10.1039/c3nr05550g
Willard MA, Kurihara LK, Carpenter EE et al (2004) Chemically prepared magnetic nanoparticles. Int Mater Rev 49:125–170. https://doi.org/10.1179/095066004225021882
Wu W, He Q, Jiang C et al (2008) Magnetic iron oxide nanoparticles: synthesis and surface functionalization strategies. Nanoscale Res Lett 3:397–415. https://doi.org/10.1007/s11671-008-9174-9
Wu X-J, Jiang R, Wu B et al (2009) Nano-iron oxide as a recyclable catalyst for intramolecular C–N cross-coupling reactions under ligand-free conditions: one-pot synthesis of 1,4-dihydroquinoline derivatives. Adv Synth Catal 351:3150–3156. https://doi.org/10.1002/adsc.200900481
Yamashita T, Hayes P (2008) Analysis of XPS spectra of Fe^{2+} and Fe^{3+} ions in oxide materials. Appl Surf Sci 254:2441–2449. https://doi.org/10.1016/j.apsusc.2007.09.063
Yang H, Ogawa T, Hasegawa D, Takahashi M (2008) Synthesis and magnetic properties of monodisperse magnetite nanocubes. J Appl Phys 103:07D526
Yang C, Wu J, Hou Y (2011) Fe_3O_4 nanostructures: synthesis, growth mechanism, properties and applications. Chem Commun 47:5130–5141
Yazdani F, Seddigh M (2016) Magnetite nanoparticles synthesized by co-precipitation method: the effects of various iron anions on specifications. Mater Chem Phys 184:318–323. https://doi.org/10.1016/J.MATCHEMPHYS.2016.09.058
Yoon S (2011) Determination of the temperature dependence of the magnetic anisotropy constant in magnetite nanoparticles. J Korean Phys Soc 59:3069–3073
Zhang B, Daigle H (2017) Oil-soluble contrast agents for NMR. In: SPWLA 58th Annual Logging Symposium, 17–21 June, Oklahoma, USA. Society of Petrophysicists and Well-Log Analysts.
Zhang X, Niu Y, Meng X et al (2013) Structural evolution and characteristics of the phase transformations between α-Fe_2O_3, Fe_3O_4 and γ-Fe_2O_3 nanoparticles under reducing and oxidizing atmospheres. CrystEngComm 15:8166–8172